IMPLEMENTATION OF INTERNAL STATE VARIABLE CONSTITUTIVE MODEL FOR FINITE ELEMENT ANALYSIS OF ROTARY FORMING PROCESSES

Elizabeth Urig, *PhD Candidate*, University of Virginia
Leonid Zhigilei, *Advisor*, University of Virginia

Abstract

Incremental spin and flow forming are promising manufacturing methods for aerospace Al alloys, though computational modeling of the deformation process is still in the developmental phase. The selection of a constitutive law, within existing finite element models, to describe the underlying material behavior affects prediction of final residual stresses, plastic strains, and part geometries. The large thermal gradients, varied strain rates, and oscillating loading characteristic of spin and flow forming require a constitutive law that accounts for thermal profile, deformation history, and work hardening behavior. The mechanical threshold stress (MTS) constitutive model is selected and derived for use in finite element spin form modeling. Initial comparison to experimental flow stress curves shows good agreement with MTS model predictions.

Introduction

Spin and flow forming are metal manufacturing processes that involve large plastic deformations. Computational research is currently ongoing to capture the residual stress, plastic straining, and deformation geometry during the forming process.[1,2] While finite element analysis efforts have made significant strides in understanding the forming process, the finite element analysis is fundamentally dependent on the underlying material description at the continuum scale. The material description, also known as the constitutive model, is a model simplifying the underlying physics of the material response based on different mechanical and thermal loading conditions. A broad range of constitutive models have been developed for various loading conditions and/or materials. Follansbee divided constitutive laws into two main categories: path dependent and path independent.[3,4] Path independent models treat strain as an internal state variable for material response evolution. The equations in these models describe the dependence of the material response on strain, strain rate, and temperature, but do not account for the work hardening and strain history, *i.e.*, the evolution of strain during the loading process. Particularly for non-monotonic loading, path independent constitutive model predictions can diverge from experimental and real-world measurements.

Figure 1 demonstrates a scenario with different strain rate histories, but the same intermediate strain, strain rate, and temperature input. Although both materials have the same intermediate point, the material response to additional loading is different. However, a path independent constitutive model would show the material as having the same response after the intermediate point.[3]

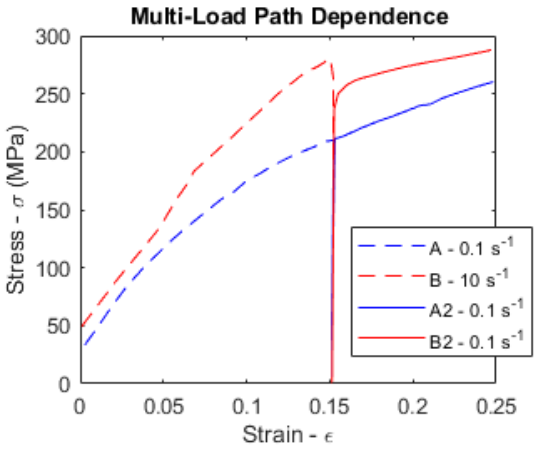

Figure 1. Two stress strain curves with different initial strain rate loading, but same secondary loading path.

Path dependent constitutive laws seek to account for the strain history by identifying a true internal state variable. Equation (1) shows the general form of the path-dependent constitutive model. One of the most common path dependent model is known as the mechanical threshold stress model. Mechanical threshold stress ($\hat{\sigma}$) is stress required to promote dislocation motion past a particular obstacle at 0 K. Since the threshold stress is rooted in the kinematics of dislocation and obstacle motion, it can capture the material response through complex loading paths more accurately than path independent models.

$$\sigma = f(\hat{\sigma}, \dot{\epsilon}, T) \qquad (1)$$

It has been shown in simulations of friction stir welding that results obtained with the MTS constitutive model are within 2% of the experimental measurements, while the predictions made with path independent methodologies show deviations over 15% for varied load cycling inputs.[5]

Methodology

Spin Forming Load Paths

The purpose of this work was to determine the characteristic load path conditions of spin forming and identify and derive an appropriate constitutive model for the spin forming loads. Previous work has gone into the development of a finite element model suitable for spin forming.[6] Both literature results and the model predictions show that the loading has a clear cyclic behavior, with cycles occurring with the periodicity of the rotation speed.[7] Figure 2, adopted from Xu et al., shows how a roller loading generates regions of tension and compression in the plastic zone surrounding the roller contact.[7]

As the roller precesses around the material, a given region will undergo cyclic loading of alternating compression and tension stages. Therefore, based on the alternating loads, spin and flow form continuum modeling would benefit from path-dependent constitutive models.

Mechanical Threshold Stress

The mechanical threshold stress constitutive model is a set of equations which determine the stress response of a material based on the mechanical threshold stress ($\hat{\sigma}$), strain rate ($\dot{\epsilon}$), and temperature (T). The stress response is determined through two master curves which characterize the MTS associated with the material saturation stress and the hardening rule based on Voce theory.[4,5] Equations (2)-(6) list the master curves and dependencies.

$$\sigma = \sigma_a + s(\dot{\epsilon}, T)\hat{\sigma} \qquad (2)$$

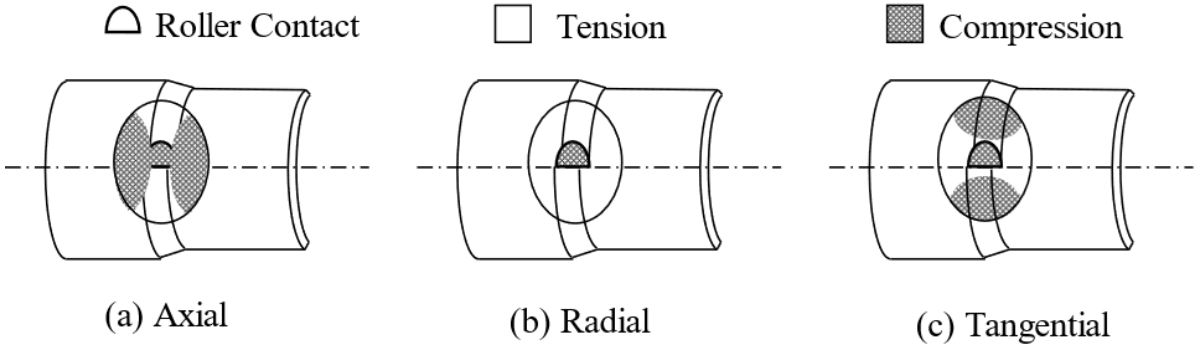

Figure 2. Regions of tension and compression within the plastic zone of an applied roller load during flow forming, adapted from Xu et al.[7]

$$\frac{\sigma}{\mu(T)} = \frac{\sigma_a}{\mu(T)} + s_\epsilon(\dot{\epsilon}, T)\frac{\widehat{\sigma_\epsilon}(\epsilon, \dot{\epsilon}, T)}{\mu_0} \quad (3)$$

$$s_\epsilon(\dot{\epsilon}, T) = \left\{\left[1 - \frac{kT}{\mu b^3 g_o}\ln\left(\frac{\dot{\epsilon_0}}{\dot{\epsilon}}\right)\right]^{\frac{1}{q}}\right\}^{\frac{1}{p}} \quad (4)$$

$$\frac{d\widehat{\sigma_\epsilon}}{d\epsilon} = \Theta_{II}\left(1 - \frac{\hat{\sigma}_\epsilon}{\widehat{\sigma_V}(\dot{\epsilon}, T)}\right) \quad (5)$$

$$ln\,\widehat{\sigma_V}(\dot{\epsilon}, T) = ln\,\widehat{\sigma_{V0}} + \frac{kT}{\mu b^3 g_0} ln\left(\frac{\dot{\epsilon}}{\dot{\epsilon_0}}\right) \quad (6)$$

Equation (2) is the governing equation of the model, where the stress (σ) is defined as the sum of the contributions of the athermal stress (σ_a) and the temperature and strain rate dependent ($s(\dot{\epsilon}, T)$) contribution of the mechanical threshold stress ($\hat{\sigma}$). Equation (3) is an extension of Equation (2), where the temperature dependence on shear stress ($\mu(T)$) is removed ($\mu_0 = \mu|_{T=0K}$). The subscript ϵ indicates the contribution of deformation and microstructure evolution to the mechanical threshold stress. Of note, additional terms of $s_a(\dot{\epsilon}, T)\widehat{\sigma_a}$ can be added to Equation (3) to account for strengthening mechanism a to the final strength.

The dependence of σ_ϵ on the evolution of microstructure, temperature, and strain rate is given by Equation (4), where k is the Boltzmann constant, b is the Burgers vector, g_0 is the activation energy required for the microstructure evolution, and $\dot{\epsilon_0}$, p, q are constants obtained from literature describing the jerky glide obstacle motion of dislocations.

The microstructure evolution is described by the Voce hardening law, outlined in Equations (5) and (6). The change in the mechanical threshold stress with respect to strain is determined by the hardening rate (Θ_{II}) and the ratio of the current threshold stress to the Voce saturation stress ($\widehat{\sigma_V}(\dot{\epsilon}, T)$). The temperature and strain rate dependent Voce stress is defined by Equation (6), where σ_{V0} is a material-specific constant initial value.

Further details of the MTS model can be found in *Fundamentals of Strength* by Paul Follansbee.[4]

For any alloy of interest, the master curves can be obtained through data manipulation of stress-strain curves obtained at multiple discrete strain rates and temperatures. In this work, a representative database of Al 6061-O flow stress curves was used.[8] The 10 strain rate and temperature test combinations are plotted in Figure 3 and Figure 4. From the 10 different stress curves, saturation stress and hardness curves can be determined.

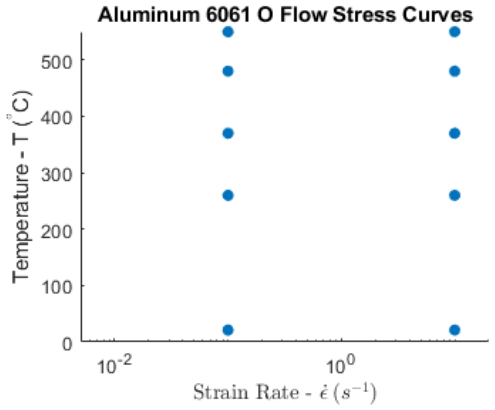

Figure 3. Strain rate and temperature combinations obtained from Battelle.[8]

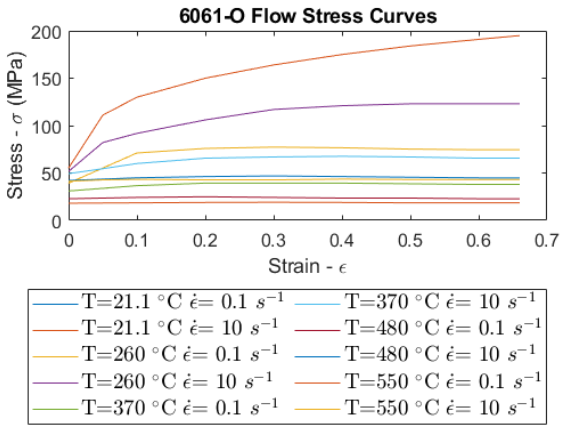

Figure 4. Flow stress curves from Battelle.[8]

Material-specific equation constants needed for equations (2)-(5) include $\mu, \dot{\epsilon_0}, b,$ and k. Equation (7) and parameters listed in Table 1 describe the temperature dependence of the shear modulus μ.

$$\mu = \mu_0 - \frac{D_0}{\exp\frac{T_0}{T+273} - 1} \quad (7)$$

The athermal portion of the stress (σ_a) is determined by plotting the yield stress against temperature, and curve fitting the asymptote. A combination of data from Al 6061-O and cast 6061 were used to estimate a lower bound for the athermal stress using a power law line of best fit. The temperature dependent experimental points and the plotted equation ($\sigma_y = 1.935 \cdot 10^{11} T^{-3.8} + 5.682$) are shown in Figure 5. The athermal stress is taken to be 5.682 MPa (Table 1).

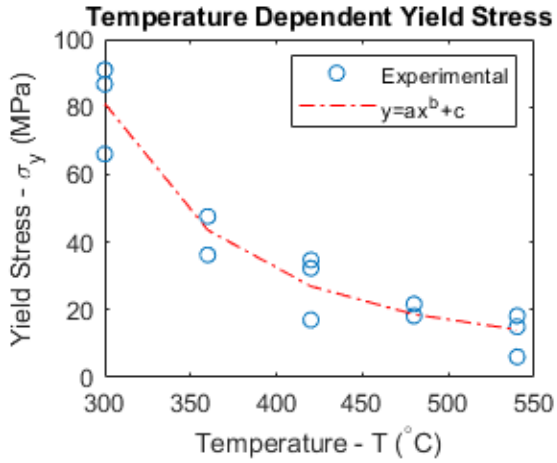

Figure 5. Temperature dependent yield stress for Al 6061 cast and annealed.

Table 1. Shear modulus parameters and athermal stress obtained for aluminum datasets.[4,9]

Parameter	Value
μ_0	28.82 GPa
D_0	3.44 GPa
T_0	215 K
σ_a	5.682 MPa

A hardening rate is determined by plotting the instantaneous stress over strain $\left(\frac{d\sigma}{d\epsilon}\right)$ against the flow stress $(\sigma - \sigma_y)$, where σ_y is the yield stress at the elastic-plastic transition. From an individual plot, such as the one shown in Figure 6, the Voce / saturation stress can be determined by the *x*-intercept of a linear fit of the type II hardening.

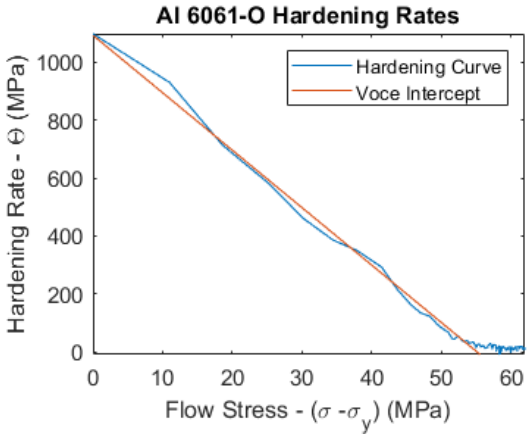

Figure 6. Hardening rate curve demonstrating Voce stress intercept location.

Once the individual saturation stress and hardening values are obtained, the master curves for Voce saturation stress and hardening rate can be determined by aggregation of the 10 different flow curves.

For the MTS algorithm, a collapsed hardening rate master curve was determined by the procedure outlined in Kuykendall and Kocks et al.[5,10] Within this procedure, the material-dependent value of the initial hardening rate at the onset of material plasticity is defined as $\left(\frac{\Theta}{\mu}\right)_0$. From ASM Handbook,[11] it is expected that for Al 6061-O this value will be in the range of the strain hardening exponent of 0.20. In the presented work, 0.17 was determined to best match the experimental range.

Beyond the hardening curves, the saturation stress master curves were based on the input

strain rate and temperature to reflect the threshold stress values. Rearranging Equation (2) into Equation (8), the linear constants (g_0 and $\left(\frac{\widehat{\sigma_{V0}}}{\mu_0}\right)^p$) can be obtained by a linear fit of the microstructure evolution curve,

$$\left(\frac{\sigma-\sigma_a}{\mu(T)}\right)^p = \left\{1-\left[\frac{kT}{g_0\mu(T)b^3}\ln\left(\frac{\dot{\epsilon}_0}{\dot{\epsilon}}\right)\right]\right\}^{1/q}\left(\frac{\widehat{\sigma_{V0}}}{\mu_0}\right)^p. \quad (8)$$

For FCC materials like aluminum, the limiting obstacle shape for dislocation movement is best described by $p = 0.5$ and $q = 1.5$.[4,5] Figure 7 shows the line of best fit (R^2 = 0.968) for the saturation stresses obtained from the flow curves shown in Figure 4.

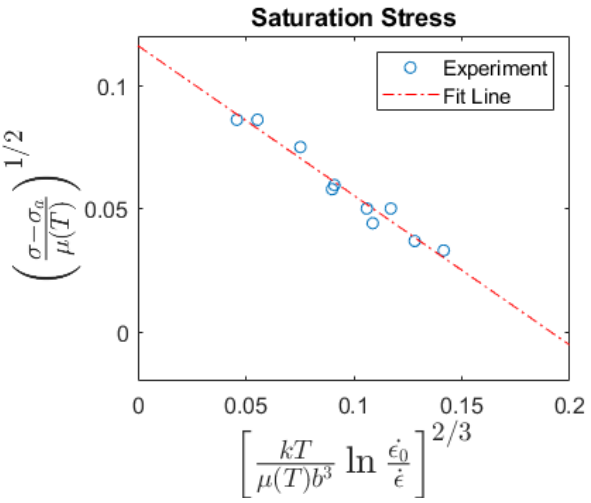

Figure 7. Master curve for saturation threshold stress

From Figure 7, we see that the set of parameters listed in Table 2 provides a good description of the microstructural evolution mechanical threshold stress and Voce saturation stress for Al 6061-O.

Table 2. MTS Constants for Al 6061-O

Parameter	Value
$\left(\frac{\Theta}{\mu}\right)_0$	0.17
b	$2.86 \cdot 10^{-10}\ m$
k	$1.380649 \cdot 10^{-23}\ J/K$
$\dot{\epsilon}_0$	$10^7 s^{-1}$
g_0	0.0947
$\frac{\widehat{\sigma_{V0}}}{\mu_0}$	0.0136

Results and Discussion

One of the main advantages of the MTS model is the ability to extrapolate to strain rates and temperatures not experimentally captured through leveraging the relationship of activation energy to temperature and strain rate. In the case of the Al 6061-O database, the strain rate and temperature ranges are 0.1 – 10 s^{-1} and 21 – 550 °C, respectively. The corresponding range of the normalized activation energy values is 0.0094 – 0.0517. If a temperature and strain rate combination yield an activation energy value within the experimental range, even if the strain rate and temperature are outside the experimental ranges of 0.1 – 10 s^{-1} and 21 – 550 °C, the MTS model can be leveraged for yield stress predictions, provided all appropriate contributions (*e.g.*, microstructural evolution, recovery, precipitates) are accounted for. The map of the activation energy g_0 evaluated for the ranges of temperature and strain rate where the MTS algorithm can accurately describe the mechanical deformation of the Al 6061-O alloy is plotted in Figure 8.

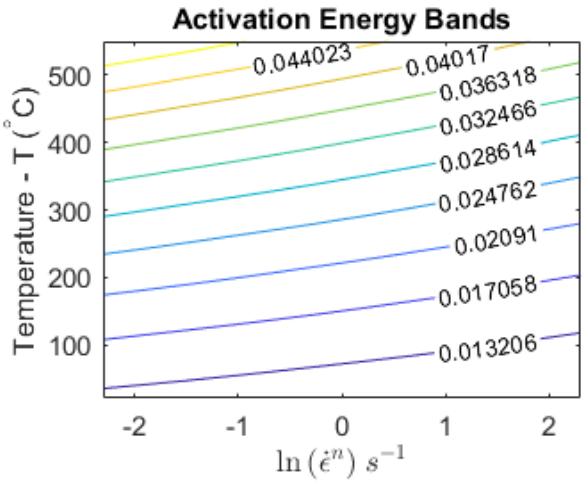

Figure 8. Al 6061-O activation energy for ranges of temperature and strain rate relevant to spin and flow forming conditions.

Using the material constants from Table 2 and Equations (2)-(6), a MATLAB script was developed to predict the MTS yield stress for a given time, strain rate, and temperature history. Figure 9 and Figure 10 show the MTS predictions for a unidirectional loading at a constant strain rate and temperature, to validate the model against experimental results. Figure 9 and Figure 10 both show generally good agreement with experiment.

To demonstrate the strain history dependence of the MTS algorithm, a material response curve is shown in Figure 11 for a material that undergoes a thermal cycle during constant strain rate (0.25 s^{-1}) loading.

The MTS algorithm was shown to match well the hardening rate of experimental flow stress curves, across multiple strain and temperature regimes. The stress curves predicted by the algorithm show remarkably good agreement at low temperatures but exhibits some divergence at higher temperatures.

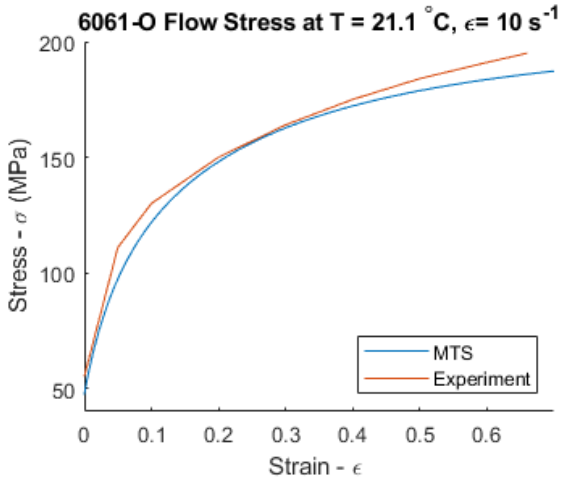

Figure 9. Room temperature flow stress curves obtained in experiment and MTS modeling.

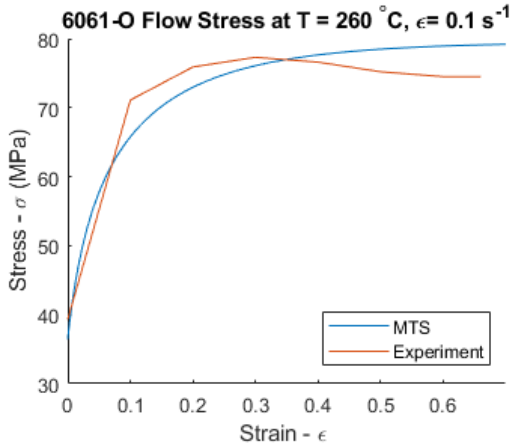

Figure 10. Elevated temperature flow stress curves obtained in experiment and MTS modeling.

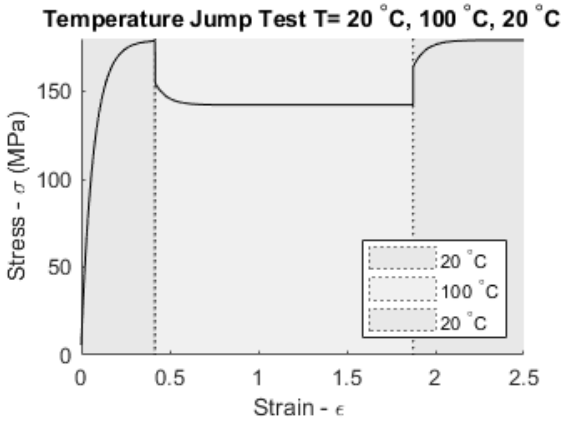

Figure 11. Temperature jump test performed with the MTS model.

The divergence indicates the material may have additional thermal effects that are not well captured by Voce hardening descriptors alone. As seen in Figure 10, the experimental flow stress reaches a peak strength around 0.3 mm/mm strain, before dropping as the test continues. The drop is characteristic of recovery, in which dislocations rearrange and annihilate as straining continues. The description of the recovery within the MTS model can be done through an addition of terms similar that used in Equation (4) to account for thermal activation.

The temperature jump test shows the power of path dependent constitutive models. The discrete steps between 20 and 100 C show a predicted lower stress at the higher temperature, which correspond to expected results. Additionally, viscous, history-dependent trends are seen at the start of the temperature transitions. The viscous behavior corresponds to the changing dislocation density and activation energy required for dislocations to move past obstacles. This behavior matches trends observed in literature.

Conclusions

The work presented shows the development of a path dependent constitutive model for spin and flow forming applications. From this work, three key conclusions can be drawn:

1. High oscillating stresses of the spin forming load paths encouraged additional development of a path dependent constitutive model for implementation within the finite element code.
2. Leveraging the MTS constitutive model offers the ability to account for the strain hardening and ensure a more accurate description of material behavior across varied loading conditions.
3. Implementation of Voce work hardening model within the MTS framework shows reasonable agreement with literature, particularly at lower temperatures.

Future Work

The development and implementation of the MTS algorithm for spin forming simulations is still ongoing. In particular, the development of additional material dislocation descriptors such as recovery and dynamic strain aging will allow for more accurate predictions across multiple obstacle regimes. Additionally, sourcing experimental thermal and strain rate jump tests will allow the MTS model to be better validated beyond that of uniaxial flow stress curves. Finally, the MTS algorithm will be implemented into DEFORM, a commercial finite element modeling software to be used for flow forming simulations.

References

[1] O. I. Bylya, M. Ward, B. Krishnamurty, S. Tamang, and R. A. Vasin, "Modelling challenges for incremental bulk processes despite advances in simulation technology: example issues and approaches," *Procedia Eng.*, vol. 207, pp. 2358–2363, 2017, doi: 10.1016/j.proeng.2017.10.1008.

[2] E. Urig and L. Zhigilei, "Finite Element Modeling of Plastic Deformation During Spin Forming of Aluminum 6061-O," presented at the VSGC 2023 Student Research Conference and Luncheon, Newport News, VA: Virginia Space Grant Consortium, Apr. 2023.

[3] P. S. Follansbee, "On the Definition of State Variables for an Internal State Variable Constitutive Model Describing Metal Deformation," *Mater. Sci. Appl.*, vol. 2014, Jun. 2014, doi: 10.4236/msa.2014.58062.

[4] P. S. Follansbee, *Fundamentals of Strength: principles, experiment, and applications of an internal state Variable Constitutive Formulation*. Wiley, Hoboken, NJ, 2014.

[5] K. L. Kuykendall, "An Evaluation of Constitutive Laws and their Ability to Predict Flow Stress over Large Variations in Temperature, Strain, and Strain Rate Characteristic of Friction Stir Welding," Dissertation, Brigham Young University, Provo, UT. [Online]. Available: https://scholarsarchive.byu.edu/etd/2768/

[6] E. Urig, K. Taminger, and L. Zhigilei, "Modeling Al-6061 Microstructural Evolution during Integrally Stiffened Cylinder Formation," presented at the 10th International Conference on Multiscale Materials Modeling, Baltimore, Oct. 20, 2022.

[7] Y. Xu, S. H. Zhang, P. Li, K. Yang, D. B. Shan, and Y. Lu, "3D rigid–plastic FEM numerical simulation on tube spinning," *J. Mater. Process. Technol.*, vol. 113, no. 1–3, pp. 710–713, Jun. 2001, doi: 10.1016/S0924-0136(01)00644-6.

[8] "Experimental Flow Stress Data," Battelle Technical Report 16, pp B-11, Nov. 1982.

[9] H. A. Kuhn, "Cast Aluminum 6061 Flow Stress Curves," National Center for Excellence in Metalworking Technology, Johnstown, PA, ADA268-301, Jan. 1991.

[10] U. F. Kocks and H. Mecking, "Physics and phenomenology of strain hardening: the FCC case," *Prog. Mater. Sci.*, vol. 48, no. 3, pp. 171–273, Jan. 2003, doi: 10.1016/S0079-6425(02)00003-8.

[11] ASM International, Ed., *ASM handbook*, 10th edition. Materials Park, Ohio: ASM International, 1990.